This article has been accepted for publication in a future issue of this journal, but has not been fully edited. Content may change prior to final publication. Citation information: DOI 10.1109/LED.2019.2898217, IEEE Electron Device Letters

Method to extract interface and bulk trap separately over the full sub-gap range in amorphous InGaZnO thin-film transistors by using various channel thicknesses

Sungju Choi, Jae-Young Kim, Jihyun Rhee, Hara Kang, Shinyoung Park, Dong Myong Kim, *Member*, *IEEE*, Sung-Jin Choi, and Dae Hwan Kim, *Senior Member*, *IEEE*

***Abstract*— We propose an experimental method to decompose the interface (insulator/channel) trap density (D_{it}) and sub-gap density-of-state (DOS) in the entire defect (g_{tot}) of amorphous InGaZnO (a-IGZO) thin-film transistors (TFTs). This method involving various active layers of different thicknesses is used for determining the origin of defects and for process optimization. These results can be used to determine clearly the contributions to the origin of the defect. Oxygen-related and deep states near the conduction band minimum (E_C) were strongly affected by the interface region. Tail states near E_C, on the other hand, were strongly influenced by the active layer. The proposed method provides physical insight and key guidelines for optimizing the performance of a-IGZO TFTs.**

***Index Terms*—Density-of-state, Interface state, InGaZnO thin-film transistor**

I. INTRODUCTION

Amorphous metal-oxide semiconductors are used as the backplanes of large-screen organic light-emitting diode (OLED) and liquid-crystal displays [1], [2]. They are also used in flexible thin-film transistors (TFTs) fabricated on plastic substrates. Amorphous InGaZnO (a-IGZO) is a popular oxide material as it has good uniformity over large areas, can be fabricated at low processing temperatures, and exhibits good device characteristics [3]. To better commercialize a-IGZO TFTs, process parameters such as the precise combination of metal cations and the hydrogen-composition ratios of the gate-insulating material and the buffer layer should be optimized. Additionally, optimized process parameters must be converted into sub-gap density-of-state (DOS) parameters that represent electrical performance. Therefore, many researchers have proposed a DOS-extraction method based on parameters such as the transient current [4], drain current [5], or multi-frequency *C*-*V* [6]. However, most researchers have extracted DOS data along with the interface-trap density (D_{it}). Even if the decomposed D_{it} is extracted separately, the states near the valance band (E_V), which is associated with reliability, are usually ignored because the defect states near E_V cannot be easily extracted [7]–[9]. Moreover, in recent times, the active thickness (T_{act}) is reduced to achieve high performance and stability [10], [11]; as a result, joint engineering has become increasingly important. Therefore, there is a demand for a method for separating and extracting D_{it} and DOS information over the full sub-gap range.

In this paper, we introduce a method that quantitatively decomposes D_{it} and DOS in entire defects of the full sub-gap range by using a photonic *C*-*V* method; these defects may have different origins [12]. Our experimental techniques are easily applicable and do not require elaborate characterization equipment. The separate extraction of thickness-independent DOS and D_{it} can be used to infer defect origin, optimize the fabrication process, and determine the quantitative contribution of each component.

II. EXPERIMENTAL PROCEDURE

The fabrication procedure of bottom-gate IGZO TFTs was described in a previous study [13]. To summarize, a-IGZO TFTs (width/length = 50/50 μm) were DC-sputter-deposited (3 kW) at room temperature with various sputter times (T_{act} = 30 nm, 50 nm, 100 nm, 150 nm, and 200 nm).

To extract D_{it} and DOS data, the transistor characteristics for various T_{act} values were measured using an Agilent 4156C precision parameter analyzer and an HP 4284A LCR meter. For each current–voltage (*I*–*V*) measurement, V_{GS} was swept from -15 to +15 V, while V_{DS} was fixed at 0.1 V. The total defect density (g_{tot}) was extracted using the monochromatic-photonic-capacitance-voltage technique; details of the methodology are available in literature [12]. Capacitance was measured by an LCR meter using a 50-kHz AC signal with 5 mW blue illumination. The *I*–*V* and $C_{g\text{-}ds}$–*V*

Manuscript received December XX, 2018. This work was supported by the National Research Foundation of Korea (NRF) grant funded by the Korea government (Ministry of Education, Science and Technology, MEST) (Nos. 2016R1A5A1012966 and 2017R1A2B4006982). The CAD software was supported by SILVACO and IDEC. The authors would like to thank Enago (www.enago.co.kr) for the English language review. The review of this letter was arranged by Editor. (Corresponding author: Dae Hwan Kim.)

S. Choi, J. Kim, J. Rhee, H. Kang, S. Park, D. M. Kim, S.-J. Choi, and D. H. Kim are with the School of Electrical Engineering, Kookmin University, Seoul 02707, Korea. (email: drlife@kookmin.ac.kr)

0741-3106 (c) 2018 IEEE. Personal use is permitted, but republication/redistribution requires IEEE permission. See http://www.ieee.org/publications_standards/publications/rights/index.html for more information.

This article has been accepted for publication in a future issue of this journal, but has not been fully edited. Content may change prior to final publication. Citation information: DOI 10.1109/LED.2019.2898217, IEEE Electron Device Letters

characteristics of devices with various T_{act} values are shown in Figs. 1(a), (b), (c), and (d). The initial V_T and subthreshold swing (*SS*) values increased and mobility decreased with increasing T_{act}. These electrical parameters were degraded by the total number of localized states as T_{act} increased.

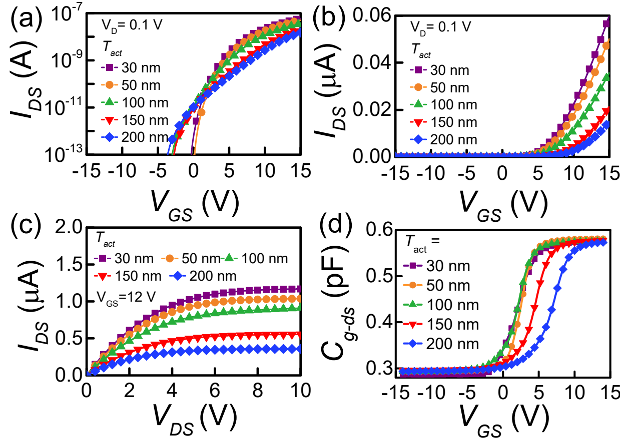

Fig. 1. Transfer in (a) semi-log scale, (b) linear scale, (c) output characteristics, and (d) *C-V* of IGZO TFTs with various T_{act}s.

III. Results and Discussions

Note that $g_{tot}(E)$ is a combination of several components of different natures; examples of these components are metal cation disorder, oxygen-related defect, and interface state, as shown Fig. 2(a). Fig. 2 shows the decomposition of g_{tot} (E) into D_{it} and g_{DOS}. The extracted g_{tot} value decreased with increasing T_{act}; hence, D_{it} must be considered. As the thickness of the channel increases, the number of defects in the channel increases, but D_{it} does not. Assuming that the DOS is uniform across the active layer, we established a piecewise model, as shown Fig. 2. (b).

$$g_{tot} = g_{DOS} + D_{it}/T_{act} \quad \left(\mathrm{eV^{-1}cm^{-3}}\right) \tag{1}$$

$$g_{tot} \cdot T_{act} = g_{DOS} \cdot T_{act} + D_{it} \quad \left(\mathrm{eV^{-1}cm^{-2}}\right) \tag{2}$$

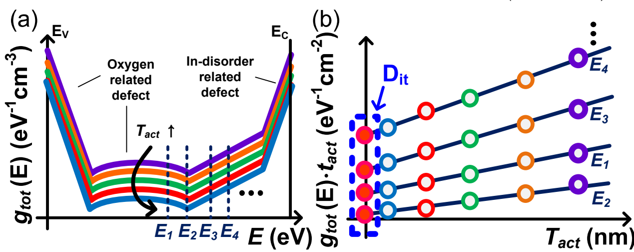

Fig. 2. (a) g_{tot} versus energy for various T_{act}s. (b) Schematic illustrating the method to separate D_{it} and DOS.

In addition, consideration of partially and fully depleted modes is essential when applying the above assumption. The depletion width (W_{dep}) was calculated by using the following equation.

$$W_{dep} = \sqrt{2 \cdot \varepsilon_{IGZO} \cdot \left(V_{bi} - V_G\right) / q \cdot n_s} \tag{3}$$

Here, ε_{IGZO} is the dielectric constant of IGZO; V_{bi} is the built-in potential in the active layer; q is the electronic charge (1.6×10^{-19} C); and n_s is the doping concentration (1×10^{16} cm^{-3}). Therefore, we can use our core assumptions up to t_{act} = 350 nm.

The extracted g_{tot} profiles for various T_{act} values are shown in Fig. 3. The measured g_{tot} values are divided into four components according to their energy-level-distribution: donor-like tail states and characteristics (g_{TD}, D_{it_TD}, kT_{TD}, and kT_{it_TD}), excess-oxygen defect states and characteristics, and center energies of the Gaussian peaks (g_{Oex}, D_{it_Oex}, kT_{Oex}, kT_{it_Oex}, E_{oex}, and E_{it_Oex}), acceptor-like deep states and characteristics (g_{DA}, D_{it_DA} kT_{DA}, and kT_{it_DA}), and tail state characteristics (g_{TA}, D_{it_TA}, kT_{TA}, and kT_{it_TA}) (in increasing order of energy levels). We modeled the extracted g_{tot} value near E_V and E_C as follows:

$$g_{TD}(E) + g_{Oex}(E) = N_{TD}\exp\left(-\frac{E-E_V}{kT_{TD}}\right) + N_{Oex}\exp\left(-\left(\frac{E-E_V-E_{Oex}}{kT_{Oex}}\right)^2\right) \tag{4}$$

$$g_{TA}(E) + g_{DA}(E) = N_{TA}\exp\left(-\frac{E_C-E}{kT_{TA}}\right) + N_{DA}\exp\left(-\frac{E_C-E}{kT_{DA}}\right) \tag{5}$$

$$D_{it,TD}(E) + D_{it,Oex}(E) = N_{it,TD}\exp\left(-\frac{E-E_V}{kT_{it,TD}}\right) + N_{it,Oex}\exp\left(-\left(\frac{E-E_V-E_{it,Oex}}{kT_{it,Oex}}\right)^2\right) \tag{6}$$

$$D_{it,TA}(E) + D_{it,DA}(E) = N_{it,TA}\exp\left(-\frac{E_C-E}{kT_{it,TA}}\right) + N_{it,DA}\exp\left(-\frac{E_C-E}{kT_{it,DA}}\right) \tag{7}$$

They are shown by the lines in Figs. 3(a)–(f). Among the g_{tot} components, g_{TD} and $D_{it,TD}$ possibly originate from the O *p*-like (occupied) valance-band edge or tail states of the a-IGZO. Moreover, g_{TA} and $D_{it,TA}$ may originate from the In-disorder in a-IGZO; g_{Oex} and $D_{it,Oex}$ are related to the $pp\sigma^*$ states after electron-capture by the peroxide [14], and the origin of g_{DA} and D_{it_DA} remains unknown. After multiplying T_{act} by g_{tot} at a specific energy level using equation. (2), we can obtain D_{it} and the thickness-independent DOS, as shown Figs. 4(a)–(d) and Table I.

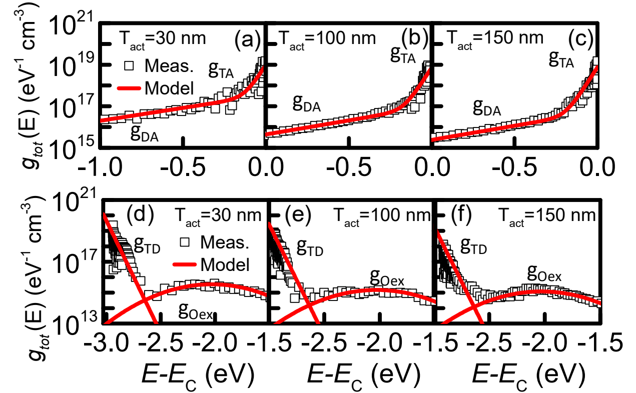

Fig. 3. Extracted g_{tot} distributions in the IGZO TFTs near E_C with T_{act} = (a) 30 nm, (b) 100 nm, and (c) 150 nm, and near E_V with T_{act} = (d) 30 nm, (e) 100 nm, and (f) 150 nm.

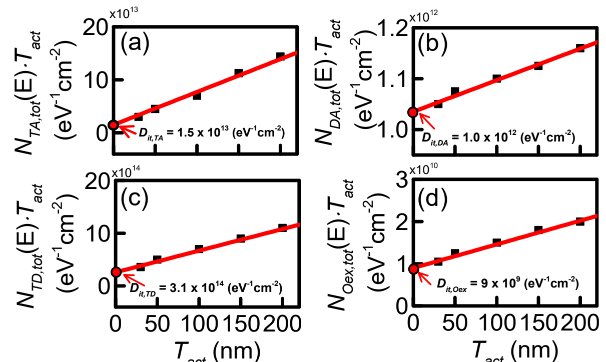

Fig. 4. Extraction method and values of D_{it} components((a) $D_{it,TA}$, (b) $D_{it,DA}$, (c) $D_{it,TD}$, and (d) $D_{it,Oex}$) for various T_{act}s.

0741-3106 (c) 2018 IEEE. Personal use is permitted, but republication/redistribution requires IEEE permission. See http://www.ieee.org/publications_standards/publications/rights/index.html for more information.

This article has been accepted for publication in a future issue of this journal, but has not been fully edited. Content may change prior to final publication. Citation information: DOI 10.1109/LED.2019.2898217, IEEE Electron Device Letters

TABLE I
EXTRACTED D_{IT} AND DOS PARAMETERS.

Parameter	g_{DOS} (eV^{-1} cm^{-3})/ D_{it} (eV^{-1} cm^{-2})	kT_{DOS}/kT_{Dit} (eV)	E_{DOS}/E_{Dit} (eV)
$g_{TA}/D_{it,TA}$	$6.0\times10^{18}/1.5\times10^{13}$	0.03 / 0.04	-
$g_{DA}/D_{it,DA}$	$3.0\times10^{16}/1.0\times10^{12}$	0.55/0.28	-
$g_{Oex}/D_{it,Oex}$	$5.0\times10^{14}/9.0\times10^{9}$	0.4/0.4	1 / 1
$g_{TD}/D_{it,TD}$	$4.0\times10^{20}/3.1\times10^{14}$	0.033/0.033	-

Both quantities were calculated at all energy points, as shown Figs. 5 (a) and (b). $D_{it,TA}$ and $D_{it,DA}$ contributed approximately 36% (7%) and 91% (63%) in the g_{tot} of the tail and the deep state, respectively, near E_C for T_{act} = 30 nm (200 nm) as shown Figs. 6(a) and (b). Further, $D_{it,TD}$ and $D_{it,Oex}$ contributed approximately 67% (24%) and 87% (50%) in the g_{tot} of the tail and excess-oxygen states, respectively, near E_V for T_{act} = 30 nm (200 nm) as shown Figs. 6(c) and (d). These results indicate that reducing T_{act} for high performance and stability [10], [11] increases the influence on D_{it}.

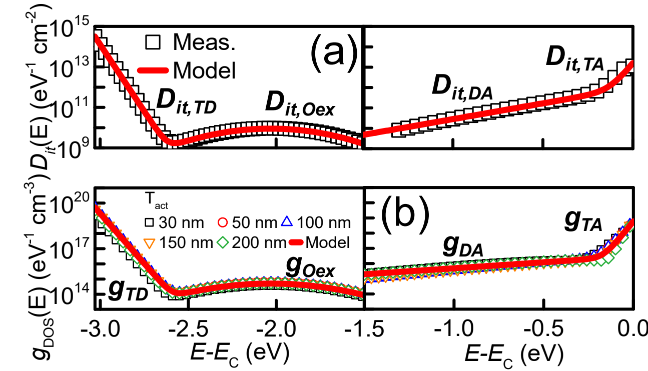

Fig. 5. (a) D_{it} and (b) g_{DOS} distributions of IGZO TFTs extracted by the proposed method.

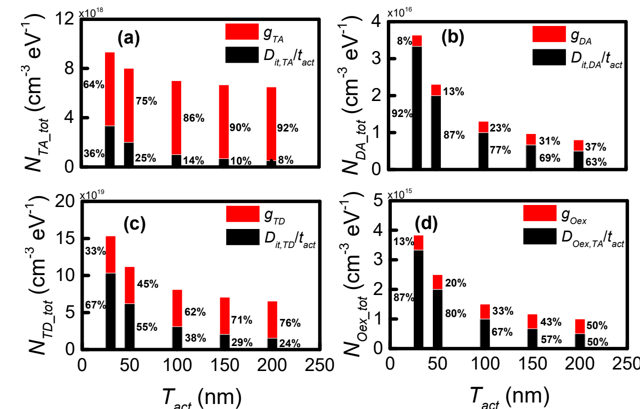

Fig. 6. Contributions as T_{act} of each defect in the states: (a) N_{TA_tot}, (b) N_{DA_tot}, (c) N_{TD_tot}, and (d) N_{Oex_tot}.

Furthermore, we estimated that mid-gap origin almost interface influence. In particular, there can be a vertical distribution of excess oxygen because the affinity between oxygen and Si is greater than that between oxygen and the other elements (Si-O > Ga-O > Zn-O > In-O) [15]. Therefore, there are more excess oxygen atoms in each interface than in the bulk, and this affects the excess oxygen and tail states near E_V. Additionally, we can infer that the deep state near E_C may be attributed to an additional coupling between Si, metal cations, and oxygen. However, the most of the states in the tail part near E_C originates from bulk defects (In-disorder defect). In addition, the extracted values are similar to previous studies [7], [9], [16]. Furthermore, to validate each extracted value, we simulated the *I-V* curves with the extracted D_{it} and the thickness-independent DOS to reproduce the experimental results for all the considered thickness values (Fig. 7(a)–(f)) [17].

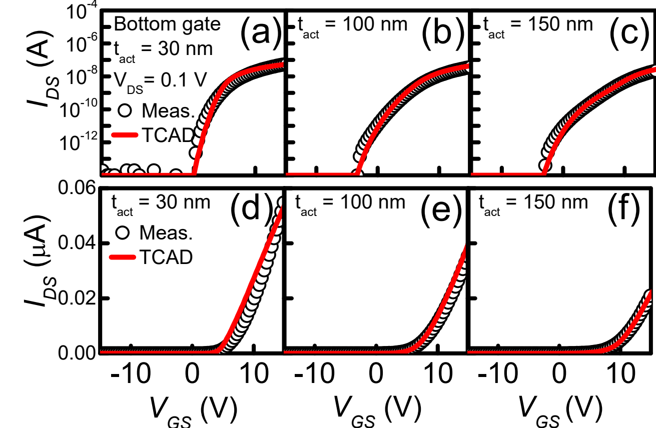

Fig. 7. Experimental and simulated *I-V* curves for V_{GS} under V_{DS} = 0.1 V (semi-log scale: (a) 30 nm, (b) 100 nm, and (c) 150 nm; and linear scale: (d) 30 nm, (e) 100 nm, and (f) 150 nm).

For the devices used in this work, we suggest utilizing the proposed method to optimize the channel and interface quality to obtain lower mid-gap states via optimized interface fabrication and tail states via optimized bulk IGZO process for further improvement in device performance. The quantitative decomposition of all defects enables an effective assessment of the complex degradation, and provides guidelines for process-optimization efforts toward achieving performance improvement. In particular, the joint optimization of the dielectrics, the active layer, and the interfaces must be performed to enhance the stability of an a-IGZO TFTs to its limit. For considering other high-mobility metal-oxide materials, the systematic decomposition of the origins of degradation followed by theoretical study and quantitative modeling is essential for realizing physical understanding and enhancement of device stability.

IV. CONCLUSION

In summary, we propose a method for experimentally identifying all defect components of D_{it} and DOS. In particular, the mid-gap state is significantly influenced by D_{it}, whereas the tail state is dominated by DOS. Measurements under various T_{act}s were used to infer the origin of defects, optimize the process, and analyze device performance. Against the background of decreasing channel thickness in electronics, for realizing high performance and reliability, it is of utmost importance to propose a method for separating and extracting D_{it} and DOS. Additionally, the systematic decomposition of the defect origin provides an insight into a complex system of multiple physical processes that occur simultaneously; such a decomposition method can be easily applied universally to any device made of any material.

0741-3106 (c) 2018 IEEE. Personal use is permitted, but republication/redistribution requires IEEE permission. See http://www.ieee.org/publications_standards/publications/rights/index.html for more information.

This article has been accepted for publication in a future issue of this journal, but has not been fully edited. Content may change prior to final publication. Citation information: DOI 10.1109/LED.2019.2898217, IEEE Electron Device Letters

REFERENCES

[1] J. Y. Noh, D. M. Han, W. C. Jeong, J. W. Kim, and S. Y. Cha, “21-1: Development of 55” 4K UHD OLED TV Employing the Internal Gate IC with High Reliability and Short Channel IGZO TFTs,” *SID Symp. Dig. Tech. Pap.*, vol. 48, no. 1, pp. 288–290, May 2017, DOI:10.1002/sdtp.11605.

[2] Y. H. Jang, D. H. Kim, W. Choi, M.-G. Kang, K. Il Chun, J. Jeon, Y. Ko, U. Choi, S. M. Lee, J. U. Bae, K. Park, S. Y. Yoon, and I. B. Kang, “Internal Compensation Type OLED Display Using High Mobility Oxide TFT,” *SID Symp. Dig. Tech. Pap.*, vol. 48, no. 1, pp. 76–79, 2017, DOI:10.1002/sdtp.11567.

[3] K. Nomura, H. Ohta, A. Takagi, T. Kamiya, M. Hirano, and H. Hosono, “Room-temperature fabrication of transparent flexible thin-film transistors using amorphous oxide semiconductors.,” *Nature*, vol. 432, no. 7016, pp. 488–492, 2004, DOI:10.1038/nature03090.

[4] M. Dai, K. Khan, S. Zhang, K. Jiang, X. Zhang, W. Wang, L. Liang, H. Cao, P. Wang, P. Wang, L. Miao, H. Qin, J. Jiang, L. Xue, and J. Chu, “A Direct Method to Extract Transient Sub-Gap Density of State (DOS) Based on Dual Gate Pulse Spectroscopy,” *Sci. Rep.*, vol. 6, no. November 2015, p. 24096, Jun. 2016, DOI:10.1038/srep24096.

[5] S. Lee, A. Nathan, S. Jeon, and J. Robertson, “Oxygen Defect-Induced Metastability in Oxide Semiconductors Probed by Gate Pulse Spectroscopy,” *Sci. Rep.*, vol. 5, no. October, p. 14902, 2015, DOI:10.1038/srep14902.

[6] S. Lee, S. Park, S.l Kim, Y. Jeon, K. Jeon, J.-H. Park, J. Park, I. Song, C. J. Kim, Y. Park, D. M. Kim, and D. H. Kim, “Extraction of Subgap Density of States in Amorphous InGaZnO Thin-Film Transistors by Using Multifrequency Capacitance–Voltage Characteristics,” *IEEE Electron Device Lett.*, vol. 31, no. 3, pp. 231–233, Mar. 2010, DOI:10.1109/LED.2009.2039634.

[7] C.-Y. Jeong, H.-J. Kim, J. I. Kim, J.-H. Lee, and H.-I. Kwon, “Extraction of bulk and interface trap densities in amorphous InGaZnO thin-film transistors,” *J. Vac. Sci. Technol. B, Nanotechnol. Microelectron. Mater. Process. Meas. Phenom.*, vol. 34, no. 6, p. 60601, Nov. 2016, DOI:10.1116/1.4964608.

[8] C.-S. Fuh, P.-T. Liu, W.-H. Huang, and S. M. Sze, “Effect of Annealing on Defect Elimination for High Mobility Amorphous Indium-Zinc-Tin-Oxide Thin-Film Transistor,” *IEEE Electron Device Lett.*, vol. 35, no. 11, pp. 1103–1105, Nov. 2014, DOI:10.1109/LED.2014.2354598.

[9] L. Qiang and R. H. Yao, “A new extraction method of trap states in amorphous ingazno thin-film transistors,” *IEEE/OSA J. Disp. Technol.*, vol. 11, no. 4, pp. 325–329, Apr. 2015, DOI:10.1109/JDT.2014.2387378.

[10] M. M. Billah, M. D. H. Chowdhury, M. Mativenga, J. G. Um, R. K. Mruthyunjaya, G. N. Heiler, T. J. Tredwell, and J. Jang, “Analysis of Improved Performance under Negative Bias Illumination Stress of Dual Gate Driving a-IGZO TFT by TCAD Simulation,” *IEEE Electron Device Lett.*, vol. 37, no. 6, pp. 735–738, 2016, DOI:10.1109/LED.2016.2557358.

[11] M. Mativenga, J. G. Um, and J. Jang, “Reduction of Bias and Light Instability of Mixed Oxide Thin-Film Transistors,” *Appl. Sci.*, vol. 7, no. 9, p. 885, 2017, DOI:10.3390/app7090885.

[12] H. Bae, H. Choi, S. Jun, C. Jo, Y. H. Kim, J. S. Hwang, J. Ahn, S. Oh, J.-U. U. Bae, S.-J. J. Choi, D. M. D. H. Kim, and D. M. D. H. Kim, “Single-Scan monochromatic photonic capacitance-voltage technique for extraction of subgap dos over the bandgap in amorphous semiconductor tfts,” *IEEE Electron Device Lett.*, vol. 34, no. 12, pp. 1524–1526, Dec. 2013, DOI:10.1109/LED.2013.2287511.

[13] S. Choi, H. Kim, C. Jo, H.-S. Kim, S.-J. Choi, D. M. Kim, J. Park, and D. H. Kim, “The Effect of Gate and Drain Fields on the Competition Between Donor-Like State Creation and Local Electron Trapping in In–Ga–Zn–O Thin Film Transistors Under Current Stress,” *IEEE Electron Device Lett.*, vol. 36, no. 12, pp. 1336–1339, Dec. 2015, DOI:10.1109/LED.2015.2487370.

[14] S. Choi, J. Jang, H. Kang, J. H. Baeck, J. U. Bae, K.-S. Park, S. Y. Yoon, I. B. Kang, D. M. Kim, S.-J. Choi, Y.-S. Kim, S. Oh, and D. H. Kim, “Systematic Decomposition of the Positive Bias Stress Instability in Self-Aligned Coplanar InGaZnO Thin-Film Transistors,” *IEEE Electron Device Lett.*, vol. 38, no. 5, pp. 1–1, 2017, DOI:10.1109/LED.2017.2681204.

[15] S. Oh, J. H. Baeck, J. U. Bae, K. S. Park, and I. B. Kang, “Effect of interfacial excess oxygen on positive-bias temperature stress instability of self-aligned coplanar InGaZnO thin-film transistors,” *Appl. Phys. Lett.*, vol. 108, no. 14, 2016, DOI:10.1063/1.4945404.

[16] X. Wei, W. Deng, J. Fang, X. Ma, and J. Huang, “Determination of bulk and interface density of states in metal oxide semiconductor thin-film transistors by using capacitance–voltage characteristics,” *Eur. Phys. J. Appl. Phys.*, vol. 80, no. 1, p. 10103, Oct. 2017, DOI:10.1051/epjap/2017170179.

[17] *ATLAS User ' s Manual*, Silvaco, Santa Clara(CA), 2018.

0741-3106 (c) 2018 IEEE. Personal use is permitted, but republication/redistribution requires IEEE permission. See http://www.ieee.org/publications_standards/publications/rights/index.html for more information.